Water Turbidity Determination by a Satellite Imagery-Based Mathematical Equation for the Chao Phraya River

Wilaiporn Pimwiset[1], Kanita Tungkananuruk[1], Thitima Rungratanaubon[1], Pratin Kullavanijaya[2], and Chalisa Veesommai Sillberg[1*]

[1]Department of Environmental Science, Faculty of Environment, Kasetsart University, Bangkok 10900, Thailand
[2]Excellent Center of Waste Utilization and Management, Pilot Plant Development and Training Institute, King Mongkut's University of Technology Thonburi, Bangkok 10150, Thailand

ARTICLE INFO

Received: 3 Dec 2021
Received in revised: 14 Feb 2022
Accepted: 20 Feb 2022
Published online: 16 Mar 2022
DOI: 10.32526/ennrj/20/202100237

Keywords:
Environmental data and information analysis/ Sentinel-2/ Chao Phraya River/ Statistical analysis/ Remote sensing data analysis

*** Corresponding author:**
E-mail: chali-h@hotmail.com; chalisa.v@ku.th

ABSTRACT

Turbidity is a standard water quality parameter that indicates its optical property in scattering light along the column containing suspended particles. The satellite imagery information of Sentinel-2 and the Chao Phraya River turbidity data from December 2016 to February 2021 was applied to develop a mathematical equation for turbidity determination. This practical and straightforward approach eliminates some constraints of traditional laboratory analysis, which is labour-intensive and time-consuming in monitoring the entire river. Four studied steps were implemented: data pre-processing, correlating analysis of numerical turbidity and satellite image reflectance, developing the mathematic equations for turbidity estimation, and its validation of use. Four different bands (B2, B3, B4, and B8) and three selection methods were investigated; single-band, combination band, and ratio band. The obtained results depicted that the reflectance of B4 in the single-band process promoted the highest correlation with turbidity compared to the others. The reflectance in visible wavelengths increased when the turbidity of river water increased, particularly B4. The mathematical power equation was a more suitable function for evaluating turbidity than linear regression, quadratic, and exponential functions. A similar concentration was obtained for measured and estimated turbidity in the validation. This finding demonstrated the potential application of remotely sensed data to estimate river water turbidity with high capability and accuracy that adequately supports spatial data continuity acquisition.

1. INTRODUCTION

The Chao Phraya River is the main river of Thailand that begins in the North and flows through the central provinces, including Phra Nakhon Si Ayutthaya, Pathum Thani, Nonthaburi, and Bangkok, and exits into the Gulf of Thailand at Samut Prakan. The river is an essential resource of raw water for various usages along its waterways; water for daily consumption, industrial processes, livestock farming, and conserving ecosystems downstream. The quality of the Chao Phraya River's water is reflected in its relative contamination and proportion that affects sequentially human health and aquatic life involved (Sillberg et al., 2021). Therefore, the entire monitoring of river water quality is essential in developing its usage efficiently and cost-effectively delivering to end-users.

A standard water parameter that reflects its optical quality and is commonly used in water supply processes is turbidity. This parameter can easily be visualized for the initial assessment. The turbidity is the light scattering and absorbing property of water when containing suspended solids and colloidal matters, i.e., clay, silt, planktons, and other organisms (Mulliss et al., 1996). The high turbidity of river water is often found after heavy rain, run-off water and flooding (Marina et al., 2020). This high turbidity in water resources limits light transmission and dissolved oxygen, impacting consequently aquatic plants and animals (Güttler et al., 2013). Turbidity also affects

Citation: Pimwiset W, Tungkananuruk K, Rungratanaubon T, Kullavanijaya P, Sillberg CV. Water turbidity determination by a satellite imagery-based mathematical equation for the Chao Phraya River. Environ. Nat. Resour. J. 2022;20(3):297-309. (https://doi.org/10.32526/ennrj/20/202100237)

water supply systems by increasing the use of chemical agents and the amount of sludge generated. This contamination increases costs due to a higher concentration of suspended solids in raw water (Gikas and Tchobanoglous, 2009). Monitoring and evaluating turbidity are essential to perform regularly or map the waterway entirely (Alvado et al., 2021). However, the turbidity concentration is assessed experimentally using the traditional gravimetric method (Pavelsky and Smith, 2009). This chemical and indirect measurement method is helpful for point or spot information, but several aspects such as time-consumed, skilled-labour need, and cost must be considered when river water quality measurements encompass the entire distribution over a specified time (Giardino et al., 2001).

In recent years, a remote sensing data-based application is considered a beneficial method that provides significant syntrophic coverage to comprehensive information that can be applied practically to water quality monitoring. It offers direct contactless survey data from aerial and satellite images to estimate the turbidity and is used in many applications, i.e., water usage planning, water quality tracking, and situation assessment (Yunus et al., 2020). Remote sensing technology is an alternative method to assess the turbidity that increases the efficiency of measuring and assessing water quality along a river from gathering a wide range of data. This method reduces time and human resources for data collection with up-to-date information provided (Acharya et al., 2018). Several studies used remote sensing-based imagery to develop mathematical equations for water quality prediction. Various linear and nonlinear regression equations have been applied (Elhag et al., 2019; Li et al., 2020). This study applied remotely sensed multispectral satellite image reflection to develop a mathematical equation for estimating turbidity in the lower part of the Chao Phraya River. Four different mathematic functions and three expression processes of Sentinel-2 satellite imagery were systematically studied.

2. METHODOLOGY

The mathematical equation for the determination of water turbidity was developed based on the surface reflectance of remote sensing data. Satellite images were studied to determine their correlation to the experimental turbidity data set of the Cho Phraya River. Processes were implemented in four steps; (1) pre-processing of satellite image and numerical data, (2) analysis of the relationship between turbidity data and satellite image data, (3) developing mathematical equations for estimation of turbidity in the river, and (4) validating the obtained equations for estimation of turbidity entirely for the river. In Figure 1, the system design method of this study is summarized.

2.1 Source of data

Two datasets were used as input sources: satellite image and measured turbidity data. The satellite image data source was the Sentinel-2 satellite of the European Space Agency. The Sentinel-2 images (https://www.sentinel-hub.com/) were in wavelengths between 496.6-835.1 nm, specifically Band 2-Blue (B2), Band 3-Green (B3), Band 4-Red (B4), and Band 8-NIR (B8). These bands are in the visible and near-infrared spectrum, and their sensitivity appropriation to reflect suspended solids causing turbidity of river water has been reported (Neukermans et al., 2012). The scattering ability of bands was found relatively high even in clear, turbid, and chlorophyll-rich water (Gohin et al., 2020). Specifically, the red region was reported increase when sediment concentrations in the water or turbidity increased (Caballero et al., 2019). In this study, the used spatial resolution was at 10 meters. These satellite image data were collected in 29 scenes from December 2016 to February 2021. The data were used differently as input data for equation development and validation, respectively; data from December 2016 to December 2020 was used for developing mathematical equations and February 2021 for validating the process. The criteria from images data collection are specific times and locations. The selected images were recorded simultaneously as automatically measured turbidity data strictly, or less than 10 min differently, when no exact image matched each paired data.

The turbidity data of the Chao Phraya River was sourced from the water quality information system (https://rwater.mnre.go.th/) of the Office of the Environment Region 1-16, Phase 2; and automatic water quality measurement stations (http://rwc.mwa.co.th/page/home/) from the real-time water quality monitoring system of the Metropolitan Waterworks Authority. These measured turbidity data are automatic measurements from the monitoring station. There is a cycle of recording data in real-time every 10 min, following the Pollution Control Department criterion to measure the water source class 3. The level installation of the water quality sensor at

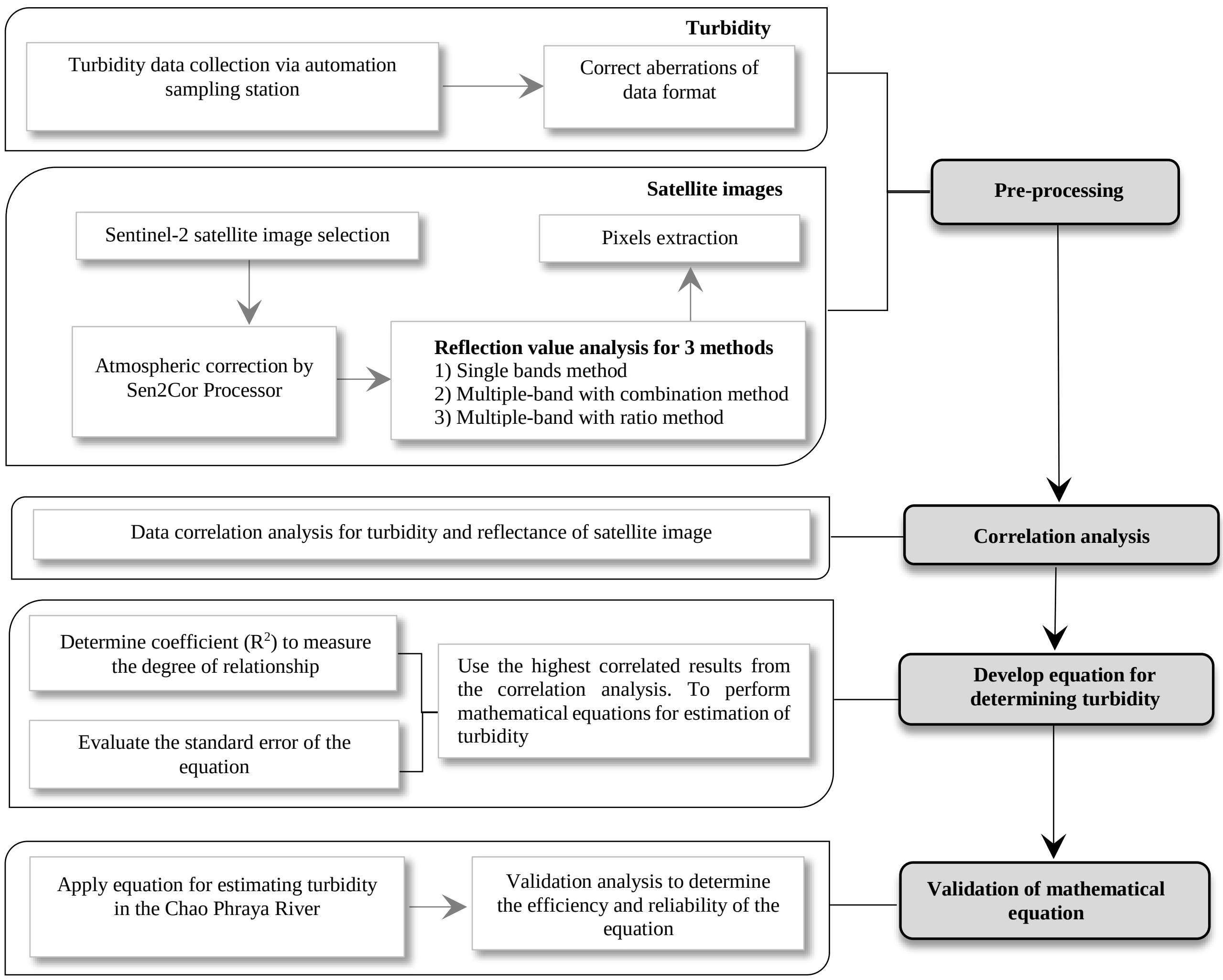

Figure 1. System design method of this study

each station is approximately 4-10 m from the bank, and the depth of the probe from the water surface to the probe is about 100-150 cm, which is below the low water level. The locations of the monitoring stations covered approximately 130 km. Geographical coordinates of the study area start at the latitude of 14.23775N, the longitude of 100.57571E, and the end coordinates of the section at the latitude of 13.54403N the longitude of 100.58935E. These monitoring stations are located at the river's width between 200-500 m. The turbidity data focused on automatic sampling installed stations at only eight stations along the lower part of Chao Phraya River, namely Saphan Krungthep; Wat Chankapo; Samlae Pathum Thani; Samut Prakan; Wat Pho Taeng Nuea, Phra Nangklao Bridge; Wat Ban Paeng; Wat Makham station. Collected data for correlation analysis were coordinates, location, date, and time of turbidity measurement and pictorial information recorded at the nearest time. Therefore, 45 data sets were obtained. The location of each water monitoring station is shown in Figure 2.

2.2 Pre-processing of satellite image and numerical data

The collected turbidity data and satellite imagery were pre-processed to correct their aberrations and eliminate incompletion and noise. There are two steps of data correction in their format, type and location between the satellite image and turbidity data.

Step 1. Fixing the turbidity data from the two data sources, numeric and imagery, into the same numeric data format. Then, showing the spatial data in the form of coordinates from the riverbank to the water quality sensor probe of the eight automatic water quality monitoring stations in the form of Point data. Moreover, set as the representative position of the water quality monitoring station to extract the reflection value in the pixel of the satellite image data to obtain data from both data sets at the same coordinate position.

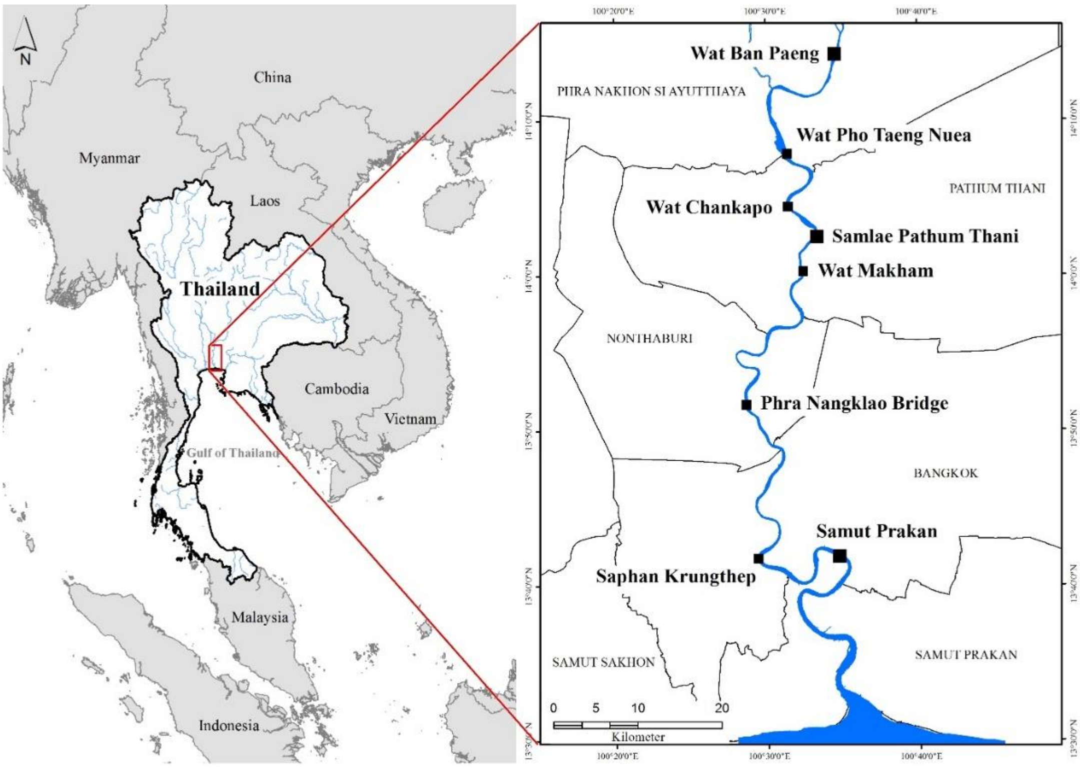

Figure 2. The study area and water quality monitoring stations of the Chao Phraya River

Step 2. Importing and correcting the satellite image data from Sentinel-2. This second step selected the paths and rows of satellite images to cover the study area and corrected aberrations due to atmospheric error correction using the Plugin Sen2Cor Processor of Sentinel Application Platform (Louis et al., 2019; Raiyani et al., 2021). Therefore, the corrected data for atmospheric error were used to analyze reflection values in multiple and single wavelengths. Then, the geographical coordinate system was corrected to define the surface water. The calculation of the reflectance value of the satellite image was conducted using three mathematical methods comparatively: Singer-band analysis, which analyzes only the reflectance values of each wavelength individually as shown as Equation (1). The multiple-band analysis was a combination method using multi-wavelength reflectance of different bands for calculation. This combination of bands is correlated well with in-situ measurements of different water quality conditions; total suspended matter, inorganic fraction, and an organic fraction (Toming et al., 2016). The additional function was applied to calculate the reflectance values from single and combined wavelengths, as shown in Equation (2). The last processing function was a multiple-band analysis. This method used the ratio of the specific band with specific wavelength reflections to calculate the reflection value by permutation between wavelengths. Therefore, the noises such as irradiance, atmospheric, and air-water surface influences in the remotely sensed signal can be minimized (Aisabokhae and Oresajo, 2018; Twumasi et al., 2019), as shown in Equation (3).

The concentration of suspended particulate matter influenced mainly the reflectance of a water body and the magnitude of the backscattering, which directly affects each band's reflectance ability (Wernand et al., 2013). Therefore, in the study, various types of reflectivity must be considered. The computational results obtained from all three methods were used to select the band processing method promoting the best correlation of imagery reflectance and turbidity data.

$$R_{rs}(\lambda)_i \tag{1}$$

$$R_{rs}(\lambda)_i + R_{rs}(\lambda)_i + , \dots + R_{rs}(\lambda)_i \tag{2}$$

$$R_{rs}(\lambda)_i \;/\; R_{rs}(\lambda)_i \tag{3}$$

Where; $R_{rs}(\lambda)_i$ is the wavelength of band n; n is the number of bands.

2.3 Correlation analysis of turbidity and satellite image data

The statistical technique was adopted in this study. An analysis via Pearson correlation coefficient was applied to perform the relative strength of correlation between measured turbidity data and satellite image data reflectance values prior to building a regression model (Li et al., 2020; Shi et al., 2018). Pearson's correlation analysis had been applied variously to examine correlation patterns between two variables. There is a tendency of correlation patterns in linear regression (Chen et al., 2020; Jayaweera and Aziz, 2018), as shown in Equation (4). The correlation coefficient was depicted as an R-value, which indicated low when it approached -1 and high when a value was closed to 1.

$$R = \frac{\sum X_i Y_i - n\bar{X}\bar{Y}}{\sqrt{\left[\sum X_i^2 - n\bar{X}^2\right]\left[\sum Y_i^2 - n\bar{Y}\right]}} \quad (4)$$

Where; X is a turbidity value in units of NTU; Y is the reflected satellite image data; i is the number of measurements 1, 2, 3,..., n.

2.4 Mathematical equations development for turbidity estimation

The results from process 2.3 were applied to develop the mathematical equations to estimate the river water turbidity. The regression analysis was implemented for linear, quadratic, power, and exponential equations, as described in Equations (5)-(8). To investigate the most suitable mathematical equation, the 95% confidence level was determined with the coefficient of determination (R^2) in a better fit condition, and a higher value was obtained.

$$Y_1 = A \times R_{rs}(\lambda) + B \quad (5)$$

$$Y_2 = A \times R_{rs}(\lambda)^2 + B \times R_{rs}(\lambda) + C \quad (6)$$

$$Y_3 = A \times R_{rs}(\lambda)^B \quad (7)$$

$$Y_4 = Ae^{B \times R_{rs}(\lambda)} \quad (8)$$

Where; A, B, and C are constant values of variables in each equation; $R_{rs}(\lambda)$ is the reflected data of the satellite image; e^B is an exponential function; λ is the wavelength of band 4; Y_1, Y_2, Y_3, and Y_4 are the estimated turbidity value from the linear regression equation, quadratic equation, power equation, and exponential equation.

The R^2 value was used to measure the degree of the relationship between the dependent and independent variables, as shown in Equation (9).

$$R^2 = \frac{\left(\sum XY - n\bar{X}\bar{Y}\right)^2}{\left(\sum X^2 - n\bar{X}^2\right)\left(\sum Y^2 - n\bar{Y}^2\right)} \quad (9)$$

Where; Y is the dependent variable; X is the independent variable; n is the number of data points

To select the appropriate equation for estimating the river's turbidity, the standard error of the estimation method was applied to the reflectance value from the satellite image data as described in Equation (10).

$$SEE = \sqrt{\frac{\sum_{i=1}^{n}(Y_i - \hat{Y})^2}{n-k-1}} \quad (10)$$

Where; SEE is the standard error of an estimation; Y is the dependent variable from equations (5), (6), (7), and (8); $\hat{Y}$ is an approximation of Y obtained from equations (5), (6), (7), and (8); n is the number of data points; k is the number of independent variables

2.5 Validation of obtained equation

The obtained mathematic equation in 2.3 was validated using satellite image information and turbidity dataset collected on February 2021 of three automatic sampling stations of the Chao Phraya River, namely Wat Ban Paeng station, Samlae Pathum Thani station, and Samut Prakan station. The equations used to calculate the reflectance of the wavelengths were compared with the measurement data.

The validation analysis of the efficiency and reliability of the equations to estimate turbidity was determined by the Root Mean Square Error (RMSE), as described in Equation (11).

$$RMSE = \sqrt{\frac{1}{n}\sum_{i=0}^{n}(\text{error})^2} \quad (11)$$

Where; error is the actual result minus the predicted result; n is the number of data points

In comparison, the results from the calibration of the turbidity data were obtained from the measurement, and the turbidity value of calculating by the reflectance in the wavelength that most closely related to the turbidity value was plotted in the Geographic information system (GIS) process, The Kriging method estimates the distance or direction between each sample point. This plot of reflected spatial relation can explain changes occurring on the surface (Ali and Ahmad, 2020).

3. RESULTS AND DISCUSSION

3.1 Pre-processed satellite image and turbidity data

This step of pre-processing satellite images and automatic collecting turbidity data was conducted to minimize the discontinuity and noise. The satellite images were recorded about 3-4 images a month. Among the studied images, a good quality condition was selected. For turbidity data, it was collected from eight automatic measurement stations that were selected by criterion condition if it had been recorded at the same date, time, and coordinates of the location that match the satellite data recording. About 28 sets of numeric data and satellite images collected from December 2016 to 2020 were studied. To sharpen the imagery, the satellite image was corrected for atmospheric discrepancies effect when recording under atmospheric conditions-comparing the satellite image data before the aberrated correcting from the normalizing position. The position used to check the reflectance after the correction was Wat Pho Taeng Nuea station (latitude 14.13939N, longitude 100.51654E), which had a lower reflectance value from the reduction of light scattering conditions. At this condition, there was now free of aerosol optical thickness and water vapour that affected the satellite image data (Fujiwara and Takeuchi, 2020) and had been reported that was the best condition in reflection ability of water bodies at the wavelength of 500-700 nm. In Figure 3, an original satellite image corrected atmospheric condition and spectrum view.

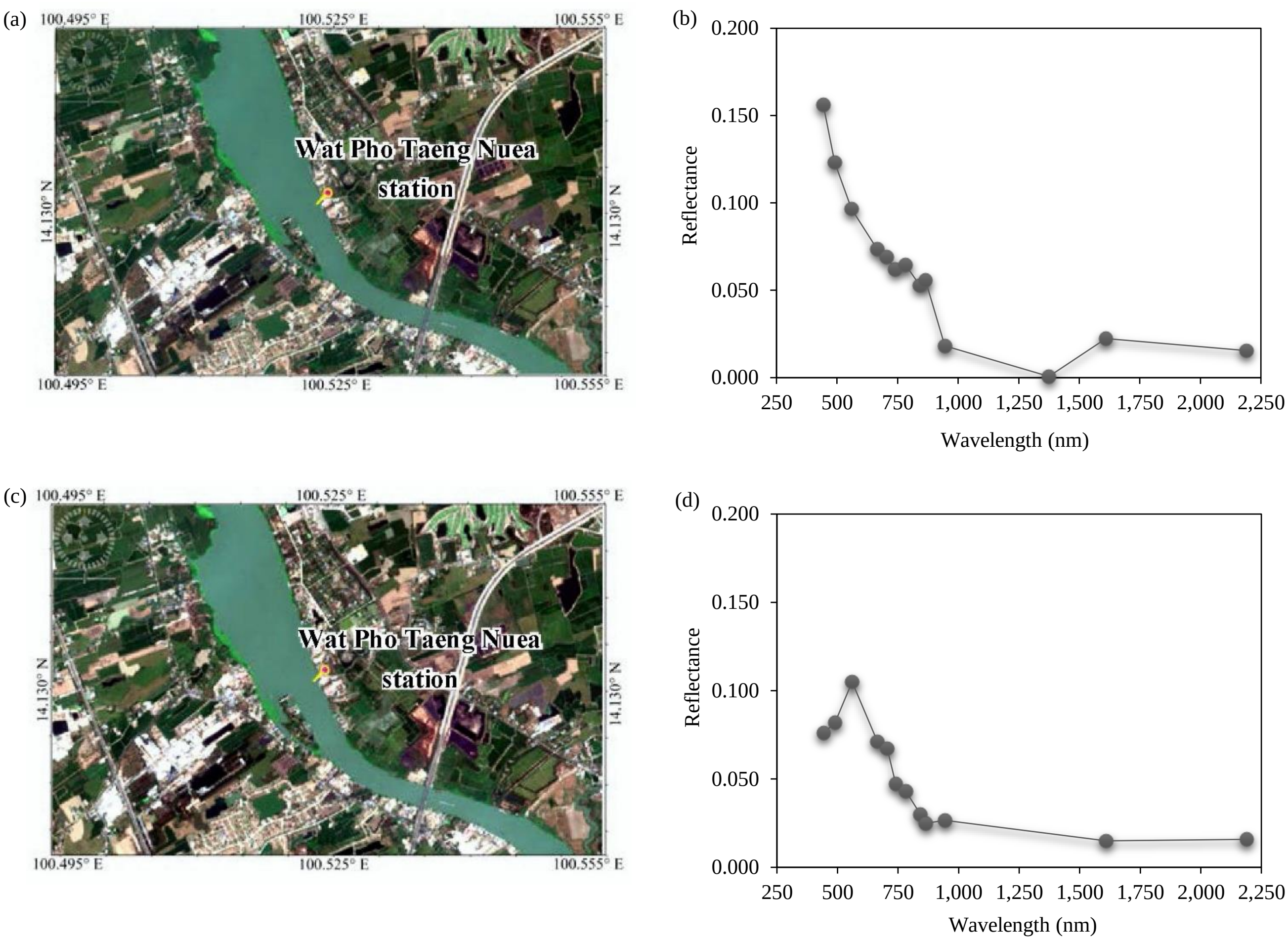

Figure 3. Top-view of satellite image and spectrum view before (a-b) and after (c-d) atmospheric correction

3.2 Correlation analysis of turbidity and reflection data of satellite image

In this step, three different conditions for the spectrum section were investigated for the correlation analysis to turbidity data. These methods were a single band, a multispectral method with a combination of wavelength, and a multispectral method with a wavelength ratio. The best correlation depicted as

Person's coefficient of band method was applied for the mathematic equation development.

3.2.1 Single-band method

The single band method uses a single wavelength, like the B2, B3, B4, and B8, in correlation with the turbidity. The obtained results depicted that spectrum B4 (central wavelength of 665 nm) was correlated maximally to turbidity concentration of the Chao Phraya River water data promoting the highest coefficient of 0.956. The following correlation was found for B3, B2, and B8 with correlation coefficients of 0.807, 0.564, and 0.146, respectively. The correlation results are provided in Table 1.

Table 1. Correlation of turbidity and satellite image reflection of single wavelength analysis

Resolution (m)	Band (B)	Correlation
		Pearson correlation
10	B2	0.564*
	B3	0.807*
	B4	0.956*
	B8	0.146**

Remark * Correlation is significant at the 0.01 level (2-tailed).
** Correlation is significant at the 0.05 level (2-tailed).

There was a significant relationship between the turbidity values in the water and the satellite image reflectance data in each wavelength. Band 4 had the best relationship because its wavelength is in visible light (red), which technically promoted the highest resolution image. Thus, better reflection values were obtained properly related significantly to the turbidity of water (Soria et al., 2017). Furthermore, this satellite provides images at 10 m resolution providing more explicit spatial information enough for relation analysis (Wang et al., 2016). It was found that the reflectance in visible light (red) increased corresponding to sediment or turbidity in the water increased. This finding was similar to the previous result (Trinh et al., 2017).

3.2.2 Multiple-band with the combination method

The second band method using a combined wavelength for relating reflectance and turbidity data was investigated. The results from multiple-band analysis indicated that the combination of band 3 and 4 (B3+B4) provided the best correlation of turbidity with the highest coefficient of 0.907, followed by bands 2 and 4 (B2+B4) and then bands 2, 4, and 3 (B2+B3+B4) with a correlation coefficient of 0.867 and 0.852, respectively, which shown as Table 2.

Table 2. Correlation of turbidity and satellite image reflection of combination method

Resolution (m)	Rating	Band (B)	Correlation
			Pearson coefficient*
10	1	B3+B4	0.907
	2	B2+B4	0.867
	3	B2+B3+B4	0.852
	4	B3+B4+B8	0.839
	5	B4+B8	0.822
	6	B2+B3+B4+B8	0.792
	7	B2+B4+B8	0.764
	8	B2+B3	0.726
	9	B3+B8	0.646
	10	B2+B3+B8	0.628

Remark * Correlation is significant at the 0.01 level (2-tailed).

It was found that multiple-band analysis based on a combination of the wavelength of B3 and B4 can identify significant relationships for turbidity and the reflectance data from satellite imagery. Those bands represent green and red colours, reflecting plant cover and chlorophyll absorption (Clevers and Gitelson, 2013). It had been reported that the visible region of the spectrum promoted an excellent correlation of reflectance and turbidity, mainly when water bodies contained high concentrations of suspended sediment particles (Garg et al., 2020). Therefore, when these two wavelengths were combined, the correlation coefficient regarding predicting water turbidity was the highest, similar to Ouma et al. (2020).

3.2.3 Multiple-band with ratio method

The results from multiple-band analysis with the ratio method indicated that the ratio between band 4 and band 3 (B4/B3) provided the best relationship or turbidity prediction with the highest correlation coefficient of 0.884, followed by bands 4 and 2 (B4/B2) and then bands 4 and 8 (B4/B8) with a correlation coefficient of 0.774 and 0.430, which shown as Table 3.

Compared to the previous method, it was found that the single band method of B4 promoted correlation efficiency of 0.956 ($p<0.01$), which is higher than the combination band method (Band 3 and Band 4; B3+B4) and multiband with ratio method (B4/B3). The result indicated data distribution model was a linear and nonlinear correlation between mathematically calculated reflection values and

Table 3. Relationship between turbidity and reflection data based on multiple-band with ratio method

Resolution (m)	Rating	Band (B)	Correlation
			Pearson coefficient
10	1	B4/B3	0.884*
	2	B4/B2	0.774*
	3	B4/B8	0.430*
	4	B3/B2	0.373**
	5	B3/B8	0.266
	6	B2/B8	0.192
	7	B8/B2	-0.136
	8	B8/B3	-0.184
	9	B8/B4	-0.331**
	10	B2/B3	-0.367**

Remark * Correlation is significant at the 0.01 level (2-tailed).
** Correlation is significant at the 0.05 level (2-tailed).

turbidity data obtained from the measurement station, as shown in Figure 4, reflected well in the B4 wavelength, which related significantly to turbidity in water (Ouma et al., 2018). This reflectance of light increased when the suspended solid increased, particularly in the visible (red) band (Vanhellemont, 2019).

3.3 Development of mathematic equation for turbidity estimation

To develop a mathematical equation for estimating river turbidity, B4 was selected as the analytical variable. This process used 45 datasets applied to four mathematical equations (linear regression, quadratic, power, and exponential mathematical equation). The mathematical power equation was the most suitable for the assessment of the turbidity because (1) the equation had a correlation coefficient (R^2) greater than 0.8; (2) the relationship was significant (p<0.01); (3) the standard error of estimates was less than for the other equations. The power equation was also the best for estimating sea-surface suspended particulate matter concentrations of the southern North Sea (Eleveld et al., 2008) and for dispersion analysis of suspended river sediment concentration (Yao et al., 2020).

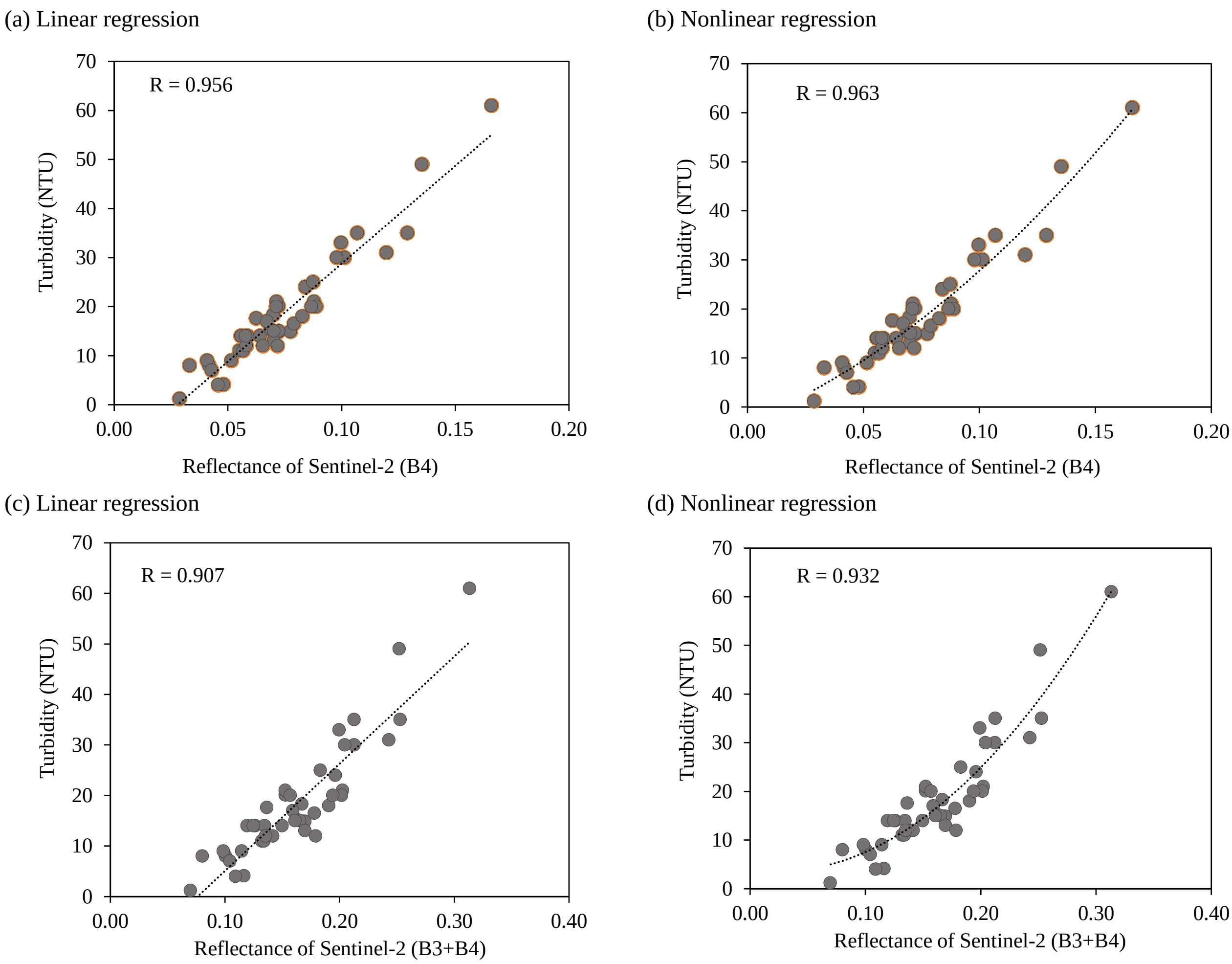

Figure 4. Linear and nonlinear regression plotted of the single-band method (a-b), multiple-band with combination method (c-d), multiple-band with ratio method (e-f)

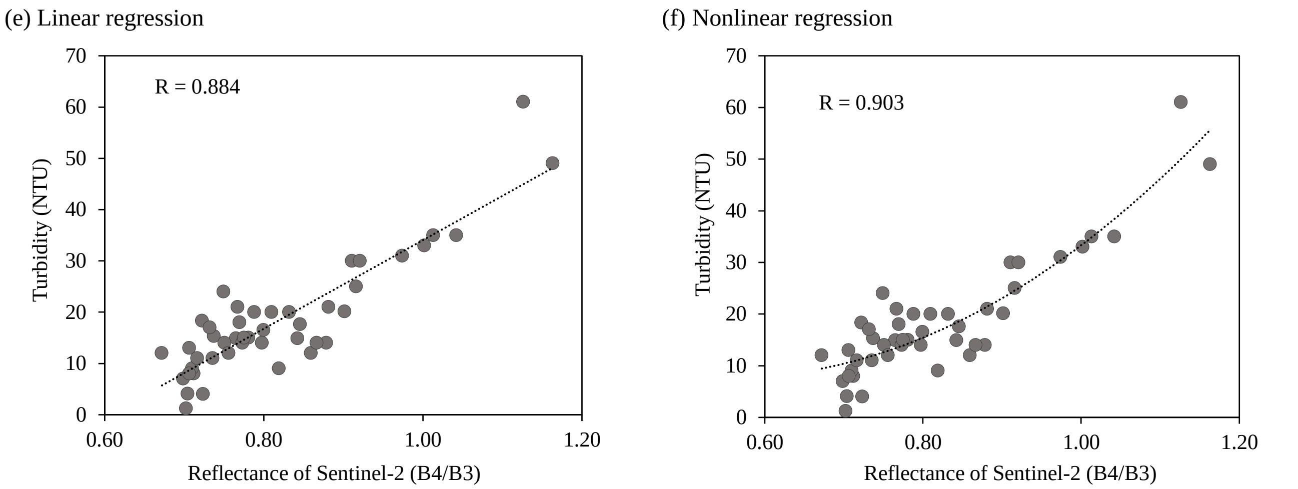

Figure 4. Linear and nonlinear regression plotted of the single-band method (a-b), multiple-band with combination method (c-d), multiple-band with ratio method (e-f) (cont.)

Linear regression is the most feasible and straightforward mathematical equation for correlation analysis, whereas quadratic and exponential equations use nonlinear regression that may be difficult in modelling, but nonlinear can explain more variation. These methods have been used to evaluate water quality (Quang et al., 2017; Sebastia-Frasquet et al., 2019). In some cases, the R^2 value may not reflect a good indicator for the accuracy of the prediction equation (Dixon, 2020; Gani et al., 2021). In this case, a standard error is considered a more suitable proportion (Li and Wong, 2001; Schumacker and Lomax, 2004). In this study, the standard error value was applied as a selecting criterion for the most suitable equation of turbidity estimation. The results are shown in Table 4.

Table 4. Model summary and parameter estimated

Dependent variable: Turbidity (NTU)									
Equation	Model summary					Parameter estimates			
	R^2	F	df1	df2	Sig.	Constant	b1	b2	Std. error of the estimate
Linear	0.913	453.565	1	43	0.00	-11.131	398.952	-	3.387
Quadratic	0.927	267.436	2	42	0.00	-2.961	191.619	1,156.961	3.142
Power	0.823	199.626	1	43	0.00	1,509.984	1.724	-	0.288
Exponential	0.727	114.474	1	43	0.00	3.182	21.173	-	0.358
The independent variable is B4.									

From the analysis, the power equation was the best at the 95% confidence level with an R^2 coefficient of 0.823, having a significant relationship ($p<0.01$) and a standard error of 0.288, which was lower than for the other equations. The distribution characteristics of the data are shown in Equation (12). It was found that the turbidity values calculated using the Power equation and the turbidity data from the measurement station were similarly ($p<0.05$).

$$\text{Turbidity (NTU)} = 1{,}509.984\ (\lambda)^{1.7241} \qquad (12)$$

Where; λ_4 is the reflected value from the B4 satellite imagery data from the Sentinel-2 satellite, it was consistent with the study by Hossain et al. (2021) using power equations to estimate turbidity in the river and using Landsat 8 satellite imagery data that had a high coefficient (R^2=0.95) and a significant correlation ($p<0.05$). The resulting equation had a high R^2 value and a standard error of 0.288, considered a low value. Comparing the result, the reflectance value via the Linear equation differed from (Suwanlertcharoen et al., 2020) a nonlinear (Power equation) calculation. The power equation could generate a minor variation of measured and estimated data properly.

3.4 Validation of mathematical equations for estimating river water turbidity

The satellite reflectance data of B4 was used to validate the mathematical equations for estimating river turbidity based on the turbidity values from turbidity stations in the Chao Phraya River obtained on February 2021, corrected aberrations due to atmospheric correction using the Plugin Sen2Cor Processor. This method was also applied for multi-wave rectification. The turbidity values calculated from remote sensing imagery compared to the ground truth data from the three water quality monitoring stations: Wat Ban Paeng, Samlae Pathum Thani, and Samut Prakan were the difference in the range 4.03-4.61 NTU. In detail, Table 5 and Figure 5 shows these validation results using the RMSE, with the predicted results being more significant than the data values from the three stations (4.03, 4.20, and 4.61 NTU, respectively). Similarly, RMSE was an appropriate measurement of accuracy that depicted the correlation between calculated and measured data (Neill and Hashemi, 2018) differently.

Table 5. Comparison of monitored and estimated turbidity by satellite image reflectance data

Location	Geographic coordinates		Turbidity (NTU)		RMSE
	Latitudes	Longitudes	Field data	Equation estimate	
Wat Ban Paeng	14.23774	100.57570	16	20.20	4.20
Samlae Pathum Thani	14.04192	100.55500	14	18.61	4.61
Samut Prakan	13.69576	100.48930	11.7	15.73	4.03

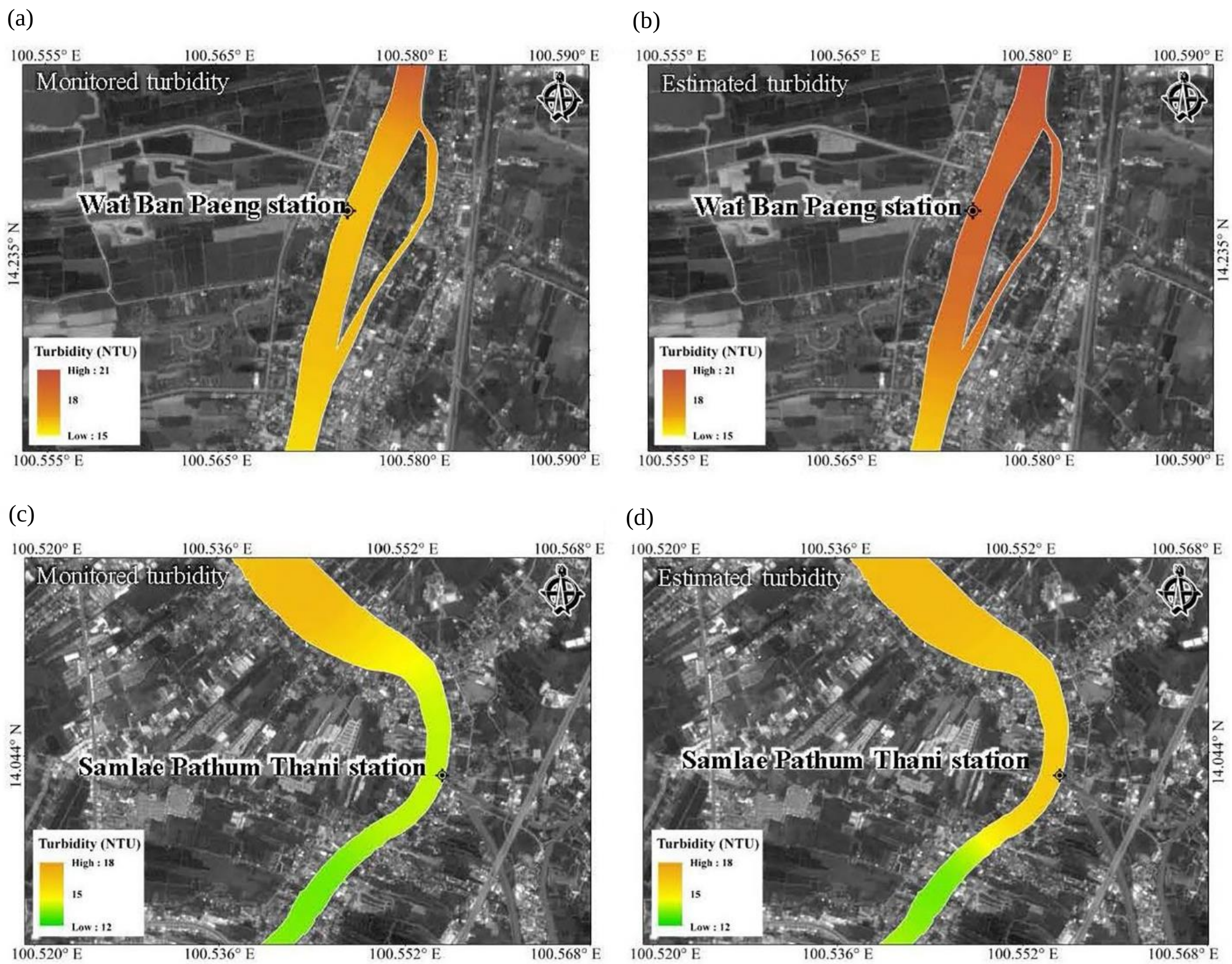

Figure 5. Monitored and estimated turbidity from the obtained equation of the Chao Phraya River at Wat Ban Paeng (a-b), Samlae Pathum Thani (c-d), and Samut Prakan (e-f) stations

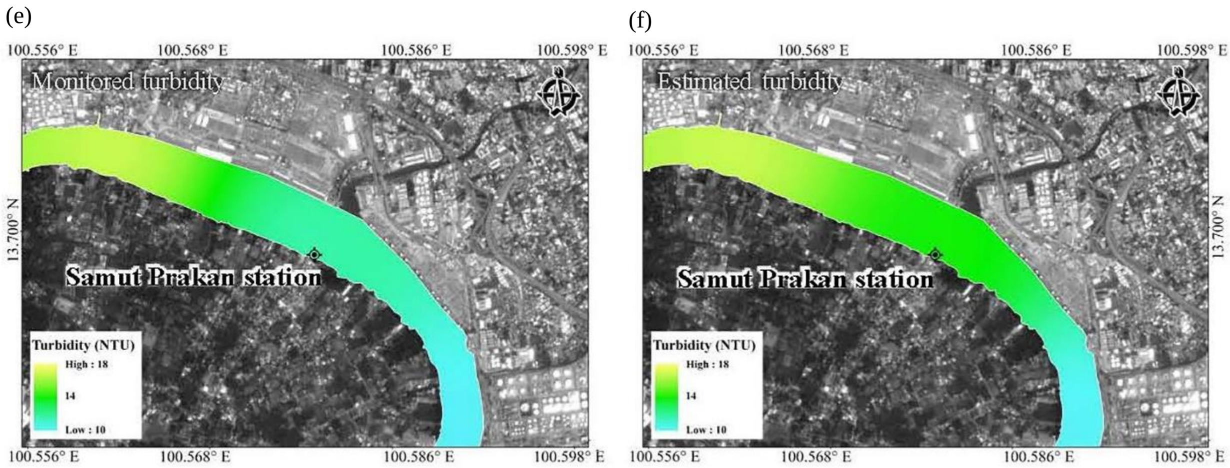

Figure 5. Monitored and estimated turbidity from the obtained equation of the Chao Phraya River at Wat Ban Paeng (a-b), Samlae Pathum Thani (c-d), and Samut Prakan (e-f) stations (cont.)

In Figure 5, the estimated turbidity using obtained equation was compared to the monitored data. It was found that the estimated turbidity of the Chao Phraya River was approximately 18-21 NTU. The higher concentration values were found at the upper part than the river's end, with about 10-16 NTU turbidity. This variation consisted of the land use characteristics around the riverbank differently in the upper through lower river part from agricultural activity and riverbank's physical characteristic, which promoted higher land deposition by the water current (Sahavacharin and Likitswat, 2019). The land use characteristics around the riverbank of the river's end were residential land use, commercial land use, and water transportation use (Ketkeaw, 2019). The flow characteristic of the water current at the end of the river decreased (Chauhan and Singh, 2020) from the decrease of transportation (Tian et al., 2021) and human activities, which beneficially disturbing less of suspended pollution in water (Collivignarelli et al., 2020; Luis et al., 2019). Consequently, the river's end turbidity was less than at the beginning and middle of the river.

From the relationship analysis between the measured turbidity and the predicted results using the three methods (single-band method, combination method, and ratio method), the single-band method with B4 produced the best relationship, with the highest correlation coefficient (0.956) as this visible band (red) is effective at indicating turbidity, as noted in the previous paragraph (Ehmann et al., 2019). It was found that the increase of sediment and turbidity levels in water sources related closely to the increase of reflectance value in the visible band (red) (Gholizadeh et al., 2016). Miller and McKee (2004) also used the visible band (red) to evaluate suspended sediment and turbidity in water sources successfully. The combination method produced the best relationship using B3 and B4 in the current study, with the highest correlation coefficient of 0.907. The ratio method revealed that the ratio between bands with the highest relationship value was between B4/B3, with a correlation coefficient of 0.884. Many studies have indicated that the ratio between the red and green visible bands could be used to assess turbidity or suspended solids (Shen et al., 2017). In the current study, river turbidity equations developed using the power equation had an R^2 value greater than 0.8 and had the lowest standard error from the four tested equations. This finding was similar to Baughman et al. (2015), who used a power equation to estimate turbidity in lakes and used the reflection value of image data from the visible band (red).

4. CONCLUSION

Retrieving turbidity of the Chao Phraya River entirely via remote sensing-based equation was developed successfully in this study. The application of reflectance band 4 in visible wavelength was correlated well with turbidity data of the river. A power equation was a suitable mathematic function fitting significantly to this correlation of satellite image reflected ability and turbidity. This estimation equation via remotely sensed data significantly benefits mapping and monitoring entire rivers by reducing the traditional process's labour-intensive, time-consuming, and analysis cost. This practical determination of water quality parameters was also valuable in providing data for planning and decision-making associated with continuous monitoring of changes in river water quality.

ACKNOWLEDGEMENTS

Author thanks the Department of Environmental Science, the Faculty of Environment, Kasetsart University, and Kasetsart University Research and Development Institute (KURDI) for the support.

REFERENCES

Acharya TD, Subedi A, Lee DH. Evaluation of water indices for surface water extraction in a Landsat 8 scene of Nepal. Sensors 2018;18(8):Article No. 2580.

Aisabokhae JE, Oresajo SB. Supervised classification of Landsat-8 band ratio images for geological interpretation of Sokoto, Nigeria. South African Journal of Geomatics 2018;7(3):360-71.

Ali SA, Ahmad A. Analysing water-borne diseases susceptibility in Kolkata Municipal Corporation using WQI and GIS based Kriging interpolation. GeoJournal 2020;85(4):1151-74.

Alvado B, Soria-Perpinya X, Vicente E, Delegido J, Urrego P, Ruiz-Verdu A, et al. Estimating organic and inorganic part of suspended solids from Sentinel 2 in different inland waters. Water 2021;13(18):Article No. 2453.

Baughman CA, Jones BM, Bartz KK, Young DB, Zimmerman CE. Reconstructing turbidity in a glacially influenced lake using the Landsat TM and ETM+ surface reflectance climate data record archive, Lake Clark, Alaska. Remote Sensing 2015;7(10):13692-710.

Caballero I, Stumpf RP, Meredith A. Preliminary assessment of turbidity and chlorophyll impact on bathymetry derived from Sentinel-2A and Sentinel-3A satellites in South Florida. Remote Sensing 2019;11(6):Article No. 645.

Chauhan A, Singh RP. Decline in PM2.5 concentrations over major cities around the world associated with COVID-19. Environmental Research 2020;187:Article No. 109634.

Chen J, Zhu W, Tian YQ, Yu Q. Monitoring dissolved organic carbon by combining Landsat-8 and Sentinel-2 satellites: Case study in Saginaw River estuary, Lake Huron. Science of the Total Environment 2020;718:Article No. 137374.

Clevers JG, Gitelson AA. Remote estimation of crop and grass chlorophyll and nitrogen content using red-edge bands on Sentinel-2 and -3. International Journal of Applied Earth Observation and Geoinformation 2013;23:344-51.

Collivignarelli MC, Abbà A, Bertanza G, Pedrazzani R, Ricciardi P, Miino MC. Lockdown for CoViD-2019 in Milan: What are the effects on air quality? Science of the Total Environment 2020;732:Article No. 139280.

Dixon MT. Exploring the Effects of Social Media Use and Avoidant Attachment Style on Marital Satisfaction and Cyber Infidelity [dissertation]. Atlanta, Mercer University; 2020.

Ehmann K, Kelleher C, Condon LE. Monitoring turbidity from above: Deploying small unoccupied aerial vehicles to image in-stream turbidity. Hydrological Processes 2019;33(6):1013-21.

Eleveld MA, Pasterkamp R, van der Woerd HJ, Pietrzak JD. Remotely sensed seasonality in the spatial distribution of sea-surface suspended particulate matter in the southern North Sea. Estuarine, Coastal and Shelf Science 2008;80(1):103-13.

Elhag M, Gitas I, Othman A, Bahrawi J, Gikas P. Assessment of water quality parameters using temporal remote sensing spectral reflectance in arid environments, Saudi Arabia. Water. 2019;11(3):Article No. 556.

Fujiwara T, Takeuchi W. Simulation of Sentinel-2 bottom of atmosphere reflectance using shadow parameters on a Deciduous Forest in Thailand. ISPRS International Journal of Geo-Information 2020;9(10):Article No. 582.

Gani A, Ion W, Yang E. Optimisation of cutting parameters and surface deformation during thin steel sheets plasma processing using Taguchi approach. Advances in Mechanical Engineering 2021;13(7):1-19.

Garg V, Aggarwal SP, Chauhan P. Changes in turbidity along Ganga River using Sentinel-2 satellite data during lockdown associated with COVID-19. Geomatics, Natural Hazards and Risk 2020;11(1):1175-95.

Gholizadeh MH, Melesse AM, Reddi L. A comprehensive review on water quality parameters estimation using remote sensing techniques. Sensors 2016;16(8):Article No. 1298.

Giardino C, Pepe M, Brivio PA, Ghezzi P, Zilioli E. Detecting chlorophyll, Secchi disk depth and surface temperature in a sub-alpine lake using Landsat imagery. Science of the Total Environment 2001;268(1-3):19-29.

Gikas P, Tchobanoglous G. The role of satellite and decentralized strategies in water resources management. Journal of Environmental Management 2009;90(1):144-52.

Gohin F, Bryère P, Lefebvre A, Sauriau P-G, Savoye N, Vantrepotte V, et al. Satellite and in situ monitoring of Chl-a, turbidity, and total suspended matter in coastal waters: Experience of the year 2017 along the French Coasts. Journal of Marine Science and Engineering 2020;8(9):Article No. 665.

Güttler FN, Niculescu S, Gohin F. Turbidity retrieval and monitoring of Danube Delta waters using multi-sensor optical remote sensing data: An integrated view from the delta plain lakes to the western-northwestern Black Sea coastal zone. Remote Sensing of Environment 2013;132:86-101.

Hossain A, Mathias C, Blanton R. Remote sensing of turbidity in the Tennessee River using Landsat 8 satellite. Remote Sensing 2021;13(18):Article No. 3785.

Jayaweera C, Aziz N. Reliability of principal component analysis and pearson correlation coefficient, for application in artificial neural network model development, for water treatment plants. IOP Conference Series: Materials Science and Engineering 2018;458:Article No. 012076.

Ketkeaw T, Thanuttamavong M, Kaveeta R. Effects of land use on water quality in Samrong Canal, Samut Prakan Province. Journal of Science and Technology 2019;21(1):175-83.

Li C, Wong WH. Model-based analysis of oligonucleotide arrays: Model validation, design issues and standard error application. Genome Biology 2001;2(8):1-11.

Li W, Niu Z, Shang R, Qin Y, Wang L, Chen H. High-resolution mapping of forest canopy height using machine learning by coupling ICESat-2 LiDAR with Sentinel-1, Sentinel-2 and Landsat-8 data. International Journal of Applied Earth Observation and Geoinformation 2020;92:Article No. 102163.

Louis J, Pflug B, Main-Knorn M, Debaecker V, Mueller-Wilm U, Iannone RQ, et al. Sentinel-2 global surface reflectance level-2A product generated with Sen2Cor. Proceedings of IEEE International Geoscience and Remote Sensing Symposium; 2019 Jul 28-Aug 2; Yokohama: Japan; 2019.

Luis KM, Rheuban JE, Kavanaugh MT, Glover DM, Wei J, Lee Z, et al. Capturing coastal water clarity variability with Landsat 8. Marine Pollution Bulletin 2019;145:96-104.

Marina P, Snezana M, Maja N, Miroslava M. Determination of heavy metal concentration and correlation analysis of turbidity: A case study of the Zlot source (Bor, Serbia). Water, Air, and Soil Pollution 2020;231(3):1-12.

Miller RL, McKee BA. Using MODIS Terra 250 m imagery to map concentrations of total suspended matter in coastal waters. Remote Sensing of Environment 2004;93(1-2):259-66.

Mulliss RM, Revitt DM, Shutes RB. The impacts of urban discharges on the hydrology and water quality of an urban watercourse. Science of the Total Environment 1996;189: 385-90.

Neill SP, Hashemi MR. Fundamentals of Ocean Renewable Energy: Generating Electricity from the Sea. London, United Kingdom, Elsevier Academic Press; 2018.

Neukermans G, Loisel H, Mériaux X, Astoreca R, McKee D. In situ variability of mass-specific beam attenuation and backscattering of marine particles with respect to particle size, density, and composition. Limnology and Oceanography 2012;57(1):124-44.

Ouma YO, Noor K, Herbert K. Modelling reservoir chlorophyll-a, TSS, and turbidity using Sentinel-2A MSI and Landsat-8 OLI satellite sensors with empirical multivariate regression. Journal of Sensors 2020;2020:Article No. 8858408.

Ouma YO, Waga J, Okech M, Lavisa O, Mbuthia D. Estimation of reservoir bio-optical water quality parameters using smartphone sensor apps and Landsat ETM+: Review and comparative experimental results. Journal of Sensors 2018;2018:Article No. 3490757.

Pavelsky TM, Smith LC. Remote sensing of suspended sediment concentration, flow velocity, and lake recharge in the Peace-Athabasca Delta, Canada. Water Resources Research 2009;45(11):Article No. W11417.

Quang NH, Sasaki J, Higa H, Huan NH. Spatiotemporal variation of turbidity based on landsat 8 oli in cam ranh bay and thuy trieu lagoon, Vietnam. Water 2017;9(8):Article No. 570.

Raiyani K, Gonçalves T, Rato L, Salgueiro P, Marques da Silva JR. Sentinel-2 image scene classification: A comparison between Sen2Cor and a machine learning approach. Remote Sensing 2021;13(2):Article No. 300.

Sahavacharin A, Likitswat F. Landscape ecological structure of Peri-Urban agricultural area in Bangkok Metropolitan Region. Journal of Community Development and Life Quality 2019;7(2);180-91.

Schumacker RE, Lomax RG. A beginner's guide to structural equation modeling. London, United Kingdom: Psychology Press; 2004.

Sebastia-Frasquet M-T, Aguilar-Maldonado JA, Santamaria-Del-Angel E, Estornell J. Sentinel 2 analysis of turbidity patterns in a coastal lagoon. Remote Sensing 2019;11(24):Article No. 2926.

Shen M, Duan H, Cao Z, Xue K, Loiselle S, Yesou H. Determination of the downwelling diffuse attenuation coefficient of lake water with the sentinel-3A OLCI. Remote Sensing 2017;9(12):Article No. 1246.

Shi L, Mao Z, Wang Z, Retrieval of total suspended matter concentrations from high resolution WorldView-2 imagery: a case study of inland rivers. IOP Conference Series: Earth and Environmental Science 2018;121(3):Article No. 032036.

Sillberg CV, Kullavanijaya P, Chavalparit O. Water quality classification by integration of attribute-realization and support vector machine for the Chao Phraya River. Journal of Ecological Engineering 2021;22(9):70-86.

Soria X, Delegido J, Urrego E, Pereira-Sandoval M, Vicente E, Ruiz-Verdu A, et al. Validación de algoritmos para la estimación de la clorofila-a con Sentinel-2 en la Albufera de València. Proceedings of the XVII Congreso de la Asociacion Espanola de Teledeteccion; 2017 Oct 3-7; Murcia, Spain; 2017.

Suwanlertcharoen T, Prukpitikula S, Buakaewa V. Retrieval of water turbidity using sentinel-2 image time series to enhance water quality assessment for consumption. Journal of Environmental Management 2020;16:74-93.

Tian X, An C, Chen Z, Tian Z. Assessing the impact of COVID-19 pandemic on urban transportation and air quality in Canada. Science of the Total Environment 2021;765:Article No. 144270.

Toming K, Kutser T, Laas A, Sepp M, Paavel B, Nõges T. First experiences in mapping lake water quality parameters with Sentinel-2 MSI imagery. Remote Sensing 2016;8(8):Article No. 640.

Trinh RC, Fichot CG, Gierach MM, Holt B, Malakar NK, Hulley G, et al. Application of Landsat 8 for monitoring impacts of wastewater discharge on coastal water quality. Frontiers in Marine Science 2017;4:Article No. 329.

Twumasi N, Shao Z, Altan O. Mapping built-up areas using two band ratio on Landsat imagery of Accra in Ghana from 1980 to 2017. Applied Ecology and Environmental Research 2019;17:13147-68.

Vanhellemont Q. Daily metre-scale mapping of water turbidity using CubeSat imagery. Optics Express 2019;27(20):1372-99.

Wang Q, Shi W, Li Z, Atkinson PM. Fusion of Sentinel-2 images. Remote Sensing of Environment 2016;187:241-52.

Wernand M, Hommersom A, van der Woerd HJ. MERIS-based ocean colour classification with the discrete Forel-Ule scale. Ocean Science 2013;9(3):477-87.

Yao R, Cai L, Liu J, Zhou M. GF-1 Satellite observations of suspended sediment injection of Yellow River Estuary, China. Remote Sensing 2020;12(19):Article No. 3126.

Yunus AP, Masago Y, Hijioka Y. COVID-19 and surface water quality: Improved lake water quality during the lockdown. Science of the Total Environment 2020;731:Article No. 139012.